Progress In Electromagnetics Research C, Vol. 43, 1–14, 2013

FAILURE MODE CHARACTERIZATION IN INKJET-PRINTED CPW LINES UTILIZING A HIGH-FREQUENCY NETWORK ANALYZER AND POST-PROCESSED TDR ANALYSIS

Sami Myllymaki[1, *], Jussi Putaala[1], Jari Hannu[1], Heli Jantunen[1], Matti Mäntysalo[2], and Esa Kunnari[3]

[1]Microelectronics and Material Physics Laboratories, University of Oulu, P. O. Box 4500, FI-90014, Finland

[2]Tampere University of Technology, P. O. Box 692, Tampere FI-33101, Finland

[3]Tampere University of Applied Sciences, Kuntokatu 3, Tampere FI-33520, Finland

Abstract—Failure mode characterization was applied to coplanar transmission lines by utilizing 0.5–10-GHz S-parameter measurements and post-calculated TDR (Time-Domain-Reflectometry) analysis. Coplanar waveguide transmission lines were inkjet-printed on 1.0-mm-thick flexible plastic RF substrates. Inductive, resistive, and capacitive types of failures — as the main failure modes caused by manufacturing, bending, or thermal cycling stresses — were investigated. The inkjet-printed CPW (Co-Planar Waveguide) lines were damaged by inductive shorts due to mechanical hitsor resistive and capacitive failures due to bending of the substrate. By using the TDR method the type and physical location of the failure can be determined.

1. INTRODUCTION

Printable electronics is a field that has received much research attention in recent years. Printable electronics utilizes widely used commercial printing processes in electronics manufacturing, enabling wide flexibility in materials, substrates, and applications with the benefit of lower costs. Inkjet printing — one of various printing technologies — is an additive and flexible fabrication method due to

Received 21 May 2013, Accepted 10 August 2013, Scheduled 21 August 2013

* Corresponding author: Sami Myllymaki (sami.myllymaki@ee.oulu.fi).

the possibility of flexibly changing digital files. It is being investigated for use in applications such as organic thin film transistors, light emitting diodes, solar cells, memories, sensors, bioactive materials and conductive structures such as printed circuit boards, antennas, microelectronic packages, and RFID (Radio Frequency Identification) tags [1–5].

The conductive layers of an inkjet-printed structure are very thin — in the order of a few micrometers — easily causing some decrements in RF performance. Thus the minimum layer thickness for minimized losses has to be at least three times the skin depth at a certain frequency. In addition the physical shape of CPW conductors has to be as rectangular as possible to avoid current jamming at the edges [6]. The electrical properties of conductive inks are determined by the size of the conductive particles, their separation in the printed and cured product, the amount of residues, etc.. In practice,the conductivity of low-temperature-cured (150°C) inks is lower than that of high-temperature-cured (850°C) inks. The conductivity of low-temperature silver inks is 20–40% compared with the conductivity of high-temperature inks. Furthermore, other electrical materials, such as dielectric and magnetic inks with low loss at high frequencies, are being developed.

The use of TDR measurement for failure analysis of electrical interconnections of BGA (Ball Grid Array) and other packaging is presented in [7–9]. The analysis involved nondestructive tests of packaged ICs and it was able to identify the location of a failure and classify open- and short-circuit defects. The accuracy of TDR measurements at 10 GHz is 50 ps, which is enough to permit detection of open or short circuits in solder ball interconnections [10]. In addition, the characteristic impedances of the central electrode with different CPW topologies were measured using the TDR method in [11]. The TDR method was able increase the level of knowledge acquired by means of the high-frequency behavior of package interconnection structures studied in [12, 13], since frequency domain results can be transformed into the time domain by using the inverse Fourier transform. To further increase measurement accuracy, the EOTPR (Electro-Optical Terahertz Pulse Reflectometry) was employed to isolate failures in advanced IC (Integrated Circuit) packages, providing 10 μm in distance accuracy at 110 GHz [14, 15].

Inkjet-printed electronics will soon face new applications operating at 1–10 GHz frequencies, e.g., in mobile telecommunications and device-to-device communications. This paper focuses on a technological evaluation of printed CPW lines used in high-frequency applications. This paper analyzes inkjet-printed CPW lines based on *S*-

parameter measurements (0.5–10 GHz) and by means of post-processed TDR results that utilize the measured S-parameters. The motivation for the paper was to validate the quality of manufactured CPW lines in RF applications. The information was based on wide band RF measurements in the frequency domain, but electrical effects are described more clearly in the time domain (i.e., post measuring analysis by using inverse Fourier transform). Moreover, the method can be applied to the manufacturing quality validation in the time domain since it's electrical realization is rather simple (i.e., preliminary validation by using oscillator and voltage level detector).

In this work, the bending of CPW lines and thermal cycling were used to induce failure modes in the structures. The results highlighted typical fault modes, their growth, and consequences observed in high-frequency signal characteristics. The CPW line structures, manufacturing process, and analyzing methodology are presented in Section 2, the experimental results and discussion are given in Section 3, and a conclusion is drawn in Section 4.

2. CPW STRUCTURE, MANUFACTURING, AND MEASUREMENT METHODOLOGY

This study was conducted on a 10-cm-long CPW line manufactured with inkjet-printing techniques as one signal conductor centered between two wide ground conductors (Fig. 1). The background was open. A failure was caused near the center of the 10-cm-long CPW line. Due to its asymmetrical location, the distance of the failure from both feed ports can be detected with different electrical characteristics. The impedance was designed to be close to 50 ohms by selecting 0.3 mm for the insulating gap and varying the center conductor from 0.2 to 0.6 mm. So, the CPW structure consisted of a homogenous transmission line without interconnections except for GSG (ground-signal-ground) probe connections at the ends of the line. A 1-mm-thick substrate of

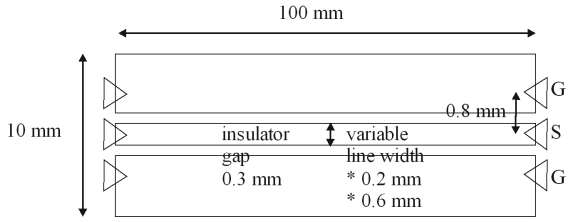

Figure 1. Schematic diagram of theCPW line structure used in the tests.

ether PPO/PPE (polyphenylene oxide/polyphenylene) from Premix Company was used in all cases. According to the manufacturer, the substrate has an ε_r value of 2.55 and a loss of 0.0005 at 1 ... 10 GHz, which are very promising loss and signal delay characteristics.

The conductors of the coplanar waveguide were fabricated using an iTi XY MDS 2.0 inkjet printer with a Spectra SE-Class drop-on-demand printhead with a 600 dpi print resolution. The printhead has 128 nozzles, and the ejected drops were ca. 30 pl in volume. Low-temperature nano-particle silver ink, NPS-JL from Harima Chemicals Inc., was used. The NPS-JL was annealed at 150°C for 60 minutes. The ink has a high silver content of 57% [16] and a relatively high resistance after thermal annealing. Before printing, the substrate was cleaned with isopropanol and treated with a 0.5% 3M$^{\text{TM}}$ Novec$^{\text{TM}}$ EGC-1720 coating. The EGC-1720 treatment decreases surface energy and increases the contact angle from 25° to 65° when the concentration of the surface treatment material ranges from 0.05% to 20%. The higher contact angle yields a smaller drop diameter and therefore narrower lines. The effect of the surface treatment on drop diameter and height was investigated in [17].

Electrical measurements of the CPW lines were performed with an Agilent 8510C network analyzer. Full 2-port calibration was performed from 500 MHz to 10 GHz by using a Cascade 106-682A substrate with ACP800 GSG probes and the LRRM (load-reflect-reflect-match) calibration method provided by Cascade. The method allows components fabricated on different substrates to be compared and ensures repeatability of the measurements. The calibrations was valid up to 18 GHz. Full 2-port S-parameter data from the CPW lines were measured and used in RF simulation software (CST Studio Suite 2011) for TDR post-processed simulations. In the TDR method an incident step pulse was generated into the system and a back-scattered voltage reflection was measured on a time scale. The shape and time of the reflected voltage can be used to determine the type of discontinuity and its location. The TDR method was applied to both ports of the measured S-parameter data of the CPW lines.

The structures were stressed in a thermal cycling test (TCT) chamber operating in a 0 ... 100°C range with 15-minute rise, fall, and dwell times, resulting in a 6.7°C/min ramp rate and one cycle per hour. The TCT adhered to JEDEC JESD22-A104 specifications.

Bending tests were done during cycling breaks; they consisted of physical bending of the CPW lines. A schematic diagram of the bending characteristics is presented in Fig. 2. To force failure modes to develop in the CPW line, the structure was bent at 45-, 75-, and 90-degree angles.

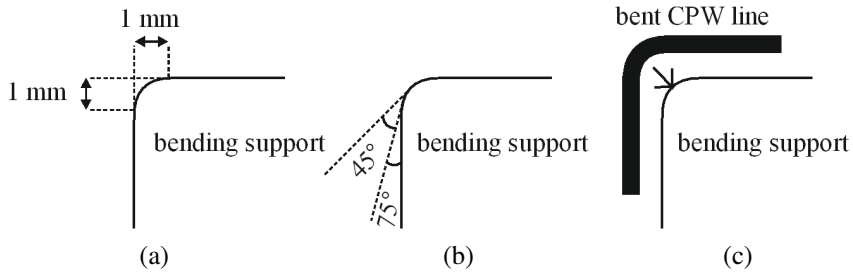

Figure 2. (a) Dimensions of the bending support used in the CPW line bending test. (b) Dimensions of bending angles of 45, 75, and 90 degrees. (c) Schematic of the bending structure with the CPW line inthe maximum bending position (90°).

Imaging of the structures was done with an optical microscope.

3. EXPERIMENTAL RESULTS AND DISCUSSION

3.1. Simulation Results

Shorted, open, or highly resistive sections are potential failures that normally appear in CPW lines. A short is an inductive failure that connects the center and ground conductors together, representing low-impedance behavior, whereas resistive and open sections represent high- and very-high-impedance behavior. All failures should fulfill theoretical signal conditions in the discontinuity presented in Fig. 3.

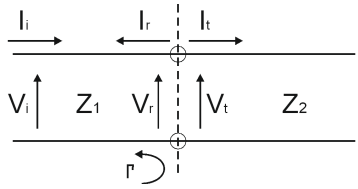

Figure 3. Transmission line discontinuity from impedance Z_1 to Z_2, V_i and I_i are representing voltage and current of incident wave, V_r and I_r reflected wave, V_t and I_t transmitted wave, and Γ is reflection coefficient.

In the discontinuity $I_i = I_r + I_t$ and $V_i + V_r = V_t$. After passing the discontinuity the energy of incident wave is divided between reflected and transmitted waves and they are passing away by their own

characteristic impedances according to the following equation:

$$\frac{V_i}{Z_1} = \frac{V_r}{Z_1} + \frac{V_t}{Z_2}. \tag{1}$$

For the reflected voltage potential we get

$$V_r = V_i \frac{Z_2 - Z_1}{Z_2 + Z_1} = \Gamma V_i. \tag{2}$$

Now we can see that if $Z_2 = Z_1$ then no reflected wave is existed, and if $Z_2 > Z_1$ then the reflected wave has the same polarity as the incident wave, and if $Z_2 < Z_1$ then the reflected wave has the opposite polarity as the incident wave. The parallel inductive failure behaves lower impedance (Z_2), and thus the reflected wave has the opposite polarity and magnitude and the voltage decreases. As a contrast, serial open and resistive failures behave higher impedances (Z_2), and thus the reflected wave has the same polarity and magnitude and the voltage increases.

Simulated TDR line impedance responses (which corresponds to voltage potential) of a simulation model of the designed 10-cm-long CPW line with shorted, open, and resistive loads in terms of signal time are presented in Fig. 4 (in the time domain). Fig. 4(a) depicts the original line, the line with a 10-µm gap (capacitive failure), and the line with a resistance (resistive failure). Both ports of the system were measured. *No discontinuity.* The homogeneous behavior of the

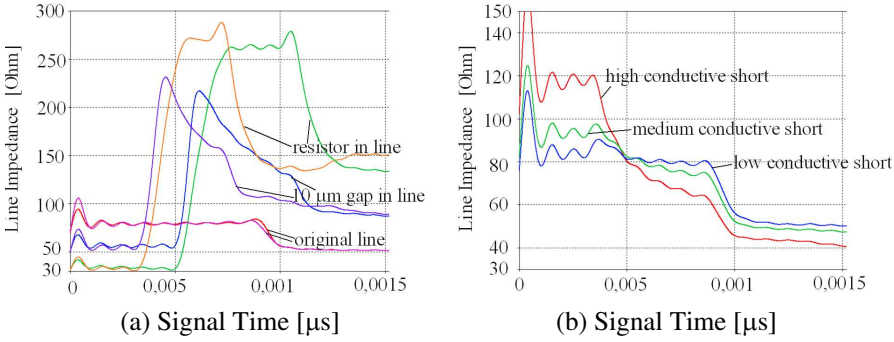

Figure 4. (a) Simulated 2-port TDR line impedance response of the 3D EM model of the original CPW line in terms of signal time with no discontinuity, with asymmetrical capacitive discontinuity, and with asymmetrical resistive discontinuity. (b) Simulated 2-port TDR line impedance response of the CPW line in terms of signal time with symmetrical inductive discontinuity.

original line produced nearly the same response at both ports when measured. The step at 0.0009 µs was caused by the opposite end (second connector) of the line. *Capacitive discontinuity.* A 10-µm gap (crack) in the line increased the line impedance up to 220 ohm at either the 0.0003 or 0.0005 µs point in time, depending on the port, and decreased evenly after the peak value. *Resistive discontinuity.* The resistance increased the impedance to 260 ohm at the 0.0003 or 0.0005 µs point. The impedance was kept high until the end of the line. After the failure, the signal level dropped in the case of a capacitive failure but remained stable in a resistive failure. *Inductive discontinuity.* The behavior of an inductive short in the middle of the CPW line is presented in Fig. 4(b). The impedance response remained rather flat when the conductivity of the short was low, and started to split into high-impedance and low-impedance sections at the 0.005 µs point when the conductivity increased.

Scattering parameter responses of the simulation model of the CPW lines are presented in Fig. 5 (in the frequency domain). In the reflection scattering responses presented in Fig. 5(a), the original line has the best characteristics, the resistive failure is hardly matched, but the open circuit is not matched at low frequencies (< 2 GHz). The transmission scattering responses in Fig. 5(b) reveal that the characteristics of open and resistive failures are close to each other at 2–10 GHz, but with 10 dB higher losses than the original line.

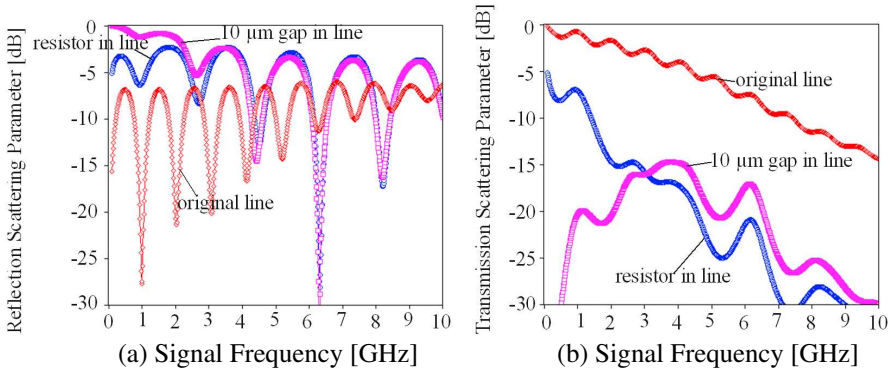

Figure 5. (a) Simulated reflection scattering response of the simulation model of the original CPW line with no discontinuity, with asymmetrical capacitive discontinuity, and with asymmetrical resistive discontinuity. (b) Simulated transmission scattering response of the simulation model of the CPW line with no discontinuity, with capacitive discontinuity, and with resistive discontinuity.

3.2. Measurement Results

Two types of CPW line failures are analyzed by using RF measurements. The first is a failure accidentally caused during the manufacturing process. A transversal cut in the substrate spreads the ink along the scratch from the ground plane to the center conductor due to capillary forces, building an arrow inductive bridge in the line (Fig. 6(a)). A similar phenomenon is described in [18]. It can be seen in the optical photo as 15-μm-wide short conductor, presented in Fig. 6(b).

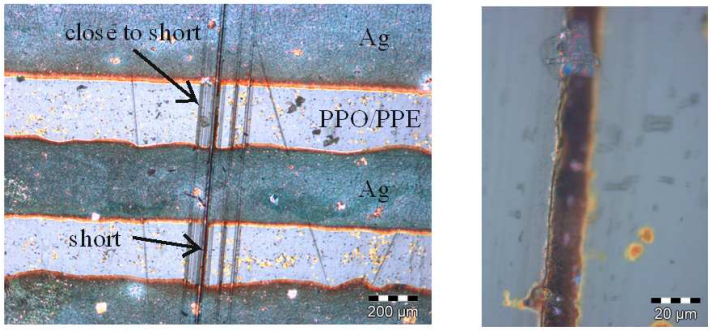

Figure 6. (a) Optical microscope photo of a damaged CPW line. A transversal cut spreads a metal neck (arrow) between the ground plane and the center line. (b) Zoomed optical microscope photo of a metal neck that connects the center line to the ground plane.

Transmissions scattering results and post-processed TDR line impedance results of a CPW line with an inductive short are presented in Fig. 7 (both frequency and time domains). The transmission scattering responses in thermal cycles up to 1000 cycles are presented in Fig. 7(a). The loss level at 1 GHz increases from a −6 dB level to −7.5 dB after 50 cycles and to −9 dB after 150 cycles. Then the loss level increases more slowly to −10 dB between 150 and 1000 cycles. At the 10-GHz frequency point the corresponding results are −11 dB, −12 dB, −13 dB, and −13.5 dB, respectively. So, the relatively detrimental effect is higher at low frequencies than at high frequencies. Post-processed TDR responses in thermal cycles up to 1000 cycles are presented in Fig. 7(b). The thermal cycling forced the TDR response to change up to 460 cycles, after which it stabilized at the level of 75 ohms in the range of 0–0.004 μs. The failure mode of the original

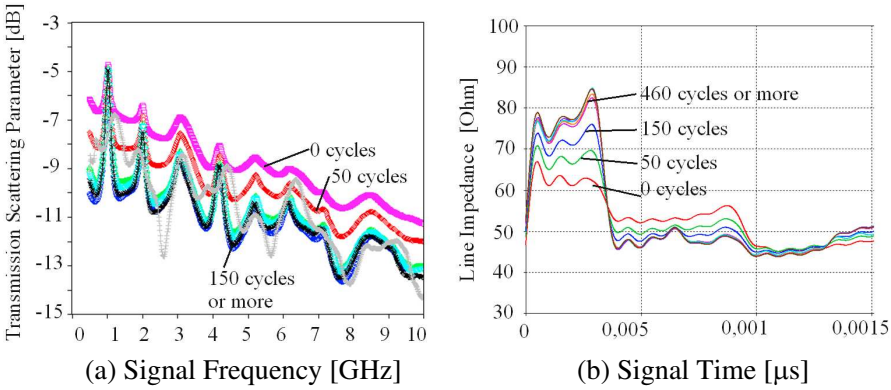

Figure 7. (a) Measured transmission scattering responses of a CPW line with an inductive short in 0–1000 thermal cycles. (b) Post-processed TDR line impedance responses of a CPW line with an inductive short in 0–1000 thermal cycles.

CPW line is straight forwardly observed from the TDR results, but not from the transmission results. The behavior of the TDR response resembles an inductance, whereas the transmission response could be caused by a different reason. The loss level in the transmission response was increased, which could be suspected to happen due to decreased conductivity of the line. However, the TDR response reveals the existence of an inductive fault. Thus, the transmission response is not decreased due to the decreased conductivity of the line but rather the increased conductivity of the fault. The characteristics are similar to theoretical characteristics of parallel inductor and the simulation results in Fig. 4(b).

The second investigated failure was caused by bending the CPW line until it started to crack mechanically. The step-by-step crack development process is presented in Fig. 8. Cracks were caused by laboratory bending (Fig. 2) in order to damage the structure mechanically at the critical level, first increasing its resistivity and finally inducing an open structure. Transmission measurements and post-processed TDR results of the CPW line with a resistive/open crack are presented in Fig. 9. Fig. 9(a) presents the transmission responses in terms of crack development and Fig. 9(b) presents the corresponding TDR responses of the damaged line. Cracks (a-b) are close to each other, crack (c) decreased the transmission response 1 dB and crack (d), 3 dB at low and high frequencies. Crack (e) drastically decreased the transmission response, and the failure mode changed from resistive to capacitive behavior, as seen from the low-frequency

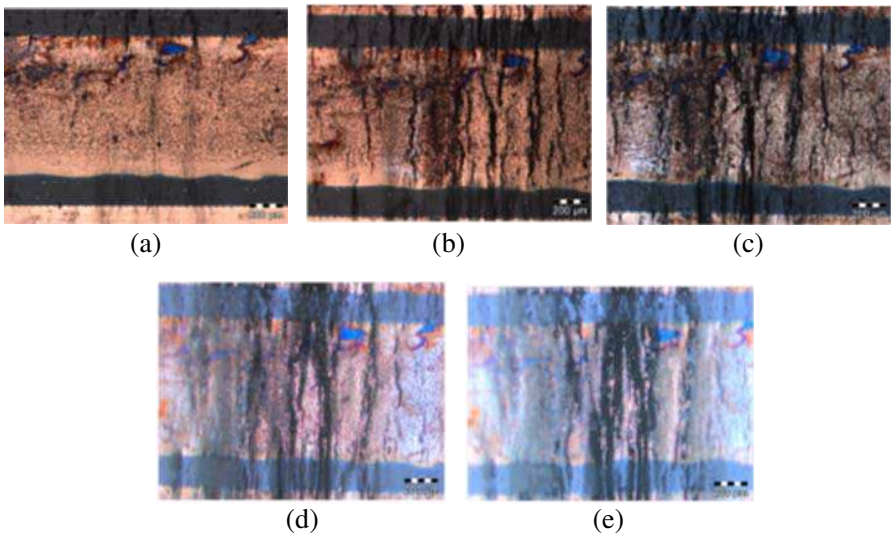

Figure 8. (a) Optical microscope photos of small cracks in a CPW line after sharp 45° bending. (b) Increased cracks after several sharp 45° bends. (c) Increased cracks after sharp 75° bending. (d) Increased cracks after sharp 90° bending, and (e) increased cracks after several sharp 75° bends.

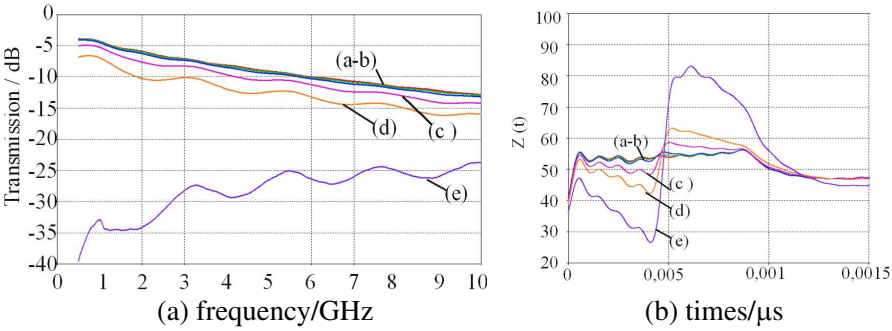

Figure 9. (a) Measured transmission response of bent CPW lines. (b) Post-processed TDR responses of bent CPW lines.

transmission response. The TDR response started to decrease in the range of 0–0.005 μs, being opposite in direction compared with the behavior that was observed with the shorted failure earlier. The characteristics are similar to theoretical characteristics of serial resistor/capacitor resembling the simulation results in Fig. 4(a).

The accuracy of the RF measurements is under ±0.1 dB which is common on-wafer error limit. The repeatability of RF measurements is even better, under ±0.05 dB. The accuracy of TDR results is varying in terms of the highest frequency and the line length. With 10 cm line the impedance step can be observed when frequency is over 5 GHz. Thus discontinues could be measured with signals operating at point frequency over 5 GHz.

The surface profiles of 200- and 600-µm-wide CPW lines are presented in Fig. 10. The 200-µm-wide line was used in shorted measurements and the 600-µm-wide line in resistive/open fault measurements. The thickness of the CPW line was 3–3.5 µm.

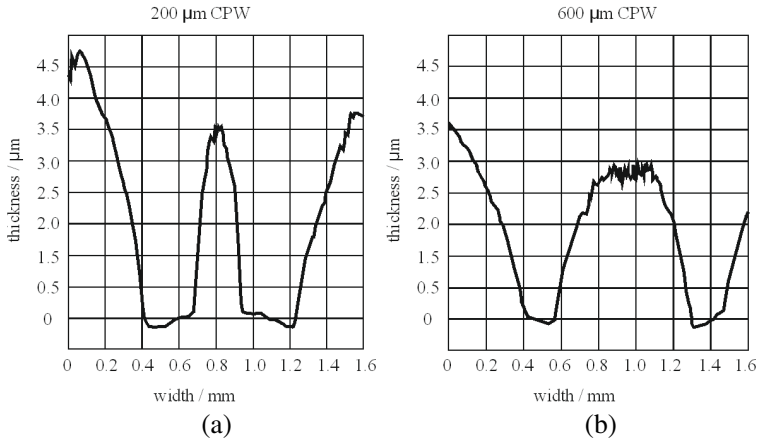

Figure 10. Measured surface profiles of (a) 200- and (b) 600-µm-wide CPW lines.

4. CONCLUSION

The technological evaluation of inkjet-printed CPW lines was presented in applications operating at radio frequencies since electronics will soon face new applications operating at 1–10 GHz frequencies, e.g., in mobile telecommunications and device-to-device communications utilizing inkjet technologies. This paper analyzed inkjet-printed CPW lines based on scattering parameter measurements (0.5–10 GHz) and by means of post-processed TDR line impedance results that utilize the measured parameters. The information was measured in frequency domain, but electrical effects were described more clearly in the time domain. The post measuring analysis was done by using the inverse Fourier transform. Coplanar waveguide transmission lines were inkjet

printed on 1-mm-thick flexible plastic RF substrates. From RF signal point of view inductive, resistive, and capacitive failures can be existed in the line. They are representing the main failure modes in a line and they have different electrical characteristics being easily observed in the time domain. Failure modes can be caused by manufacturing, bending, or thermal cycling stresses. In the paper the inkjet-printed CPW lines were damaged by inductive shorts due to mechanical hits or resistive and capacitive failures due to a bent substrate. By using the TDR method, the type and physical location of the failure can be measured. The frequency limits the accuracy. Frequencies less than 5 GHz are too inaccurate decreasing the fault resolution in the line of 10 cm. The measurement method can be applied to the manufacturing quality validation in the time domain since it's electrical realization is rather simple. The preliminary validation of lines can be realized by the feeding oscillator and detecting voltage level detector in proper applications or in manufacturing validation tests.

In this work, the bending of CPW lines and thermal cycling were used to induce failure modes in the structures. The results highlighted typical fault modes, their growth, and consequences observed in high-frequency signal and time domain characteristics.

REFERENCES

1. Pynttari, V., E. Halonen, M. Mantysalo, and R. Makinen, "The effect of sintering profile and printed layer variations with inkjet-printed large-area applications," *Electronic Components and Technology Conference (ECTC)*, 1874–1879, 2012.
2. Subramanian, V., P. C. Chang, J. B. Lee, S. E. Molesa, and S. K. Volkman, "Printed organic transistors for ultra-low-cost RFID applications," *IEEE Transactions on Components and Packaging Technologies,* Vol. 28, No. 4, 742–747, 2005.
3. Nilsson, H.-E., H. A. Andersson, A. Manuilskiy, T. Unander, K. Hammarling, J. Siden, and M. Gulliksson, "Printed write once and read many sensor memories in smart packaging applications," *IEEE Sensors Journal*, Vol. 11, No. 9, 1759–1767, 2011.
4. Gao, J., J. Siden, and H.-E. Nilsson, "Printed temperature sensors for passive RFID tags," *PIERS Proceedings*, 845–848, Xi'an, China, Mar. 22–26, 2010.
5. Trivedi, U. B., D. Lakshminarayana, I. L. Kothari, N. G. Patel, H. N. Kapse, K. K. Makhija, P. B. Patel, and C. J. Panchal, "Potentiometric biosensor for urea determination in milk," *Sensors and Actuators*, Vol. 140, No. 1, 260–266, 2009.

6. Koskinen, S., L. Pykäri, and M. Mäntysalo, "Inkjet printed flexible user interface module," *Proc. of 62nd Electronic Components and Technology Conference (ECTC)*, 1009–1014, San Diego, CA, USA, May 29–Jun. 1, 2012.
7. Pekkanen, V., M. Mäntysalo, K. Kaija, P. Mansikkamäki, E. Kunnari, K. Laine, J. Niittynen, S. Koskinen, E. Halonen, and U. Caglar, "Utilizing inkjet printing to fabricate electrical interconnections in a system-in-package," *ELSEVIER Microelectronic Engineering*, Vol. 87, No. 11, 2382–2390, 2010.
8. Mäntysalo, M. and P. Mansikkamäki, "An inkjet-deposited antenna for 2.4 GHz applications," *ELSEVIER International Journal of Electronics and Communications*, Vol. 63, 31–35, 2009.
9. Lee, H.-J., S. Seo, K. Yun, J. W. Joung, I.-Y. Oh, and J.-G. Yook, "RF performance of CPW transmission line fabricated with inkjet printing technology," *APMC Microwave Conference*, 1–4, Asia-Pacific, Dec. 16–20, 2008.
10. Chen, M.-K., C.-C. Tai, Y.-J. Huang, and I.-C. Wu, "Failure analysis of BGA package by a TDR approach," *The 4th International Symposium on Electronic Materials and Packaging,* 112–116, Dec. 4–6, 2002.
11. Abessolo-Bidzo, D., P. Poirier, P. Descamps, and B. Domengès, "Isolating failing sites in IC packages using time domain reflectometry: Case studies," *Microelectronics Reliability*, Vol. 45, Nos. 9–11, 1639–1644, 2005.
12. Kwon, D., M. H. Azarian, and M. Pecht, "Early detection of interconnect degradation by continuous monitoring of RF impedance," *IEEE Transactions on Device and Materials Reliability*, Vol. 9, No. 2, 296–304, 2009.
13. Chen, M.-K., C.-C. Tai, and Y.-J. Huang, "Non-destructive analysis of interconnection in two-die BGA using TDR," *IEEE Transactions on Instrumentation and Measurement*, Vol. 55, No. 2, 400–405, 2006.
14. Li, H.-H., J.-Y. Jao, M.-K. Chen, L.-S. Jang, and Y.-C. Hsu, "Open-ended MEMS probes for dielectric spectroscopy of biological cells at radio frequencies," *PIERS Online*, Vol. 5, No. 3, 251–255, 2009.
15. Putaala, J., T. Kangasvieri, O. Nousiainen, H. Jantunen, and M. Moilanen, "Detection of thermal cycling-induced failures in RF/microwave BGA assemblies," *IEEE Transactions on Electronics Packaging Manufacturing*, Vol. 31, No. 3, 240–247, Jul. 2008.

16. Putaala, J., O. Nousiainen, M. Komulainen, T. Kangasvieri, H. Jantunen, and M. Moilanen, "Influence of thermal-cycling-induced failures on the RF performance of ceramic antenna assemblies," *IEEE Transactions on Components, Packaging and Manufacturing Technology*, Vol. 1, No. 9, 1465–1472, 2011.
17. Tay, M. Y., L. Cao, M. Venkata, L. Tran, W. Donna, W. Qiu, J. Alton, P. F. Taday, and M. Lin, "Advanced failure isolation technique using electro-optical terahertz pulse reflectometry," *The 19th IEEE International Symposium on the Physical and Failure Analysis of Integrated Circuits (IPFA)*, 1–5, Jul. 2–6, 2012.
18. Cai, Y., Z. Wang, R. Dias, and D. Goyal, "Electro optical terahertz pulse reflectometry — An innovative failure isolation tool," *The 60th Proceedings of Electronic Components and Technology Conference (ECTC),* 1309–1315, Las Vegas, NV, USA, 2010.
19. Mäntysalo, M., L. Xie, F. Jonsson, Y. Feng, A. López Cabezas, and L.-R. Zheng, "System integration of smart packages using printed electronics," *Proc. of 62nd Electronic Components and Technology Conference (ECTC),* 997–1002, San Diego, CA, USA, May 29–Jun. 1, 2012.
20. Mäntysalo, M. and P. Mansikkamäki, "Inkjet deposited interconnections for electronic packaging," *Proceedings of IST Digital Fabrication*, 813–817, Alaska, USA, Sep. 16–21, 2007.
21. Miettinen, J., K. Kaija, M. Mäntysalo, P. Mansikkamäki, M. Kuchiki, M. Tsubouchi, R. Rönkkä, K. Hashizume, and A. Kamigori, "Molded substrates for inkjet printed module," *IEEE Transactions on Components and Packaging Technologies*, Vol. 32, No. 2, 293–301, 2009.